Int. J. Electrochem. Sci., 13 **(2018)** 2248 – 2262, doi: 10.20964/2018.03.56

International Journal of
ELECTROCHEMICAL
SCIENCE
www.electrochemsci.org

Hydrothermally-assisted co-precipitation and Electrochemical Performance of $LiNi_{1/3}Co_{1/3}Mn_{1/3}O_2$ Cathode Material

Ruixue Zhang, Liwu Huang, Wei Li, Jinyu Liao, Pan Zeng, Xinlin Zhang, Yungui Chen[*]

College of Materials Science and Engineering, Sichuan University, Chengdu 610065, PR China
[*]E-mail: ygchen60@aliyun.com

Received: 3 November 2017 / *Accepted:* 26 December 2017 / *Published:* 5 February 2018

Hydrothermally-assisted co-precipitation method is conducted to prepare the precursor of layered materials $LiNi_{1/3}Co_{1/3}Mn_{1/3}O_2$. The $LiNi_{1/3}Co_{1/3}Mn_{1/3}O_2$ cathode materials are synthesized after calcining the as-prepared precursor for different hours at 850 °C. The high-temperature and high-pressure conditions that the hydrothermal-assisted method possesses can rapidly improve the crystallization speed of $LiNi_{1/3}Co_{1/3}Mn_{1/3}O_2$ precursor also with the well-defined layer structures and low degree of cation mixing. As the result, the hydrothermally-assisted co-precipitation method can save almost half the time of precursor reaction and calcination compared with reported co-precipitation methods. At the same time, the good comprehensive electrochemical performance can be obtained with the large initial discharge capacity of 193.5 $mAh \cdot g^{-1}$ at 0.1 C (1.0 C = 183.0 $mA \cdot g^{-1}$), the capacity fading rate per cycle of only 0.016 % based on 135 cycles and the high-rate discharge ability of 126 $mAh \cdot g^{-1}$ at 4.0 C. Adopting the hydrothermally-assisted co-precipitation method is very helpful to boost the utilization of production equipments and reduce the manufacturing cost of the $LiNi_{1/3}Co_{1/3}Mn_{1/3}O_2$ material.

Keywords: hydrothermally-assisted co-precipitation; $LiNi_{1/3}Co_{1/3}Mn_{1/3}O_2$; cathode; lithium-ion battery; production process

1. INTRODUCTION

In recent years, lithium-ion batteries have been developed rapidly due to the escalation of portable electronic devices and electric vehicles. Since Goodenough et al. [1, 2] put forward layered $LiCoO_2$ as a cathode material and the Sony achieved commercial applications in 1990 [3], people also found out other cathode materials for lithium-ion batteries in succession such as $LiMn_2O_4$ [4, 5] and $LiFePO_4$ [6, 7]. $LiCoO_2$, one of the most widely used cathode materials, has good electrochemical performances and longer cycle life, but its application has been restricted due to the toxicity, safety and high cost of cobalt [8-10]. Similarly, the Jahn - Teller transition of $LiMn_2O_4$ [11, 12] and the poor

conductivity as well as low temperature performance of $LiFePO_4$ [13, 14] also prohibit their use in the future.

Many researchers make efforts to find a new kind of material which has relatively good safety performance and high specific energy. Layered material $LiNi_{1/3}Co_{1/3}Mn_{1/3}O_2$, owing to its high theoretical capacity (278.0 $mAh \cdot g^{-1}$), structural stability, safety and relatively low cost, is considered to be an ideal choice for hybrid electric vehicle (HEV) and to be the alternative of $LiCoO_2$ cathode material [15-17]. The different transition metal elements Ni, Co and Mn, existing in + 2, + 3 and + 4 valence state respectively [18], are combined together to show the synergistic effects: Co reduces the degree of cation mixing between Li^+ and Ni^{2+} in the lithium layer, Ni provides a high capacity and Mn maintains an outstanding stability of structure and reduces the cost.

In many reports, co-precipitation method is considered to be the best method for preparing spherical $LiNi_{1/3}Co_{1/3}Mn_{1/3}O_2$ materials because of the homogeneous and fine particles of precursor, especially in industry. Nonetheless, the co-precipitation method conditions must be strictly controlled and need a long time to prepare [19-21]. Park et al. [22] and Zhang et al. [23] used a carbonate co-precipitation technique to synthesize the $Ni_{1/3}Co_{1/3}Mn_{1/3}CO_3$ precursor and the latter was required to react at a constant temperature for 12 h. Santhanam et al. [24] prepared $Ni_{1/3}Co_{1/3}Mn_{1/3}(HO)_2$ precursor by a hydroxide co-precipitation at 50 °C for 20 h. More importantly, the crystallinity of precursor is unsatisfactory, resulting in longer calcination time. Park et al. [22] calcined the carbonate precursor for 20 h at 900 °C and Santhanam et al. [24] calcined the hydroxide precursor for 6 h at 400 °C and 12 h at 900 °C. It could be seen that the strict conditions and long-time reaction process were needed in these works.

Although the hydrothermal method is infrequent in the $LiNi_{1/3}Co_{1/3}Mn_{1/3}O_2$ synthesis, it is a promising process to obtain the stable electrochemical performance and improve the crystallinity of layered $LiNi_{1/3}Co_{1/3}Mn_{1/3}O_2$ [25]. High temperature and pressure of hydrothermal method in a sealed condition are helpful to improve the crystallinity of transition metal oxide cathode materials and then the lower calcination temperature and less calcination time can be adopted to save the cost and energy consumption. But the longer hydrothermal synthesizing time is still a nonnegligible problem. Wu et al. [26] synthesized $LiNi_{1/3}Co_{1/3}Mn_{1/3}O_2$ materials via hydrothermal method and the precursor reacted at 160 °C under auto-generated pressure for 30 h. After calcination for 6 h at 850 °C, the electrochemical performance was better than that of the traditional co-precipitation method.

In this work, we have succeeded in preparing layered $LiNi_{1/3}Co_{1/3}Mn_{1/3}O_2$ by the simple hydrothermally-assisted co-precipitation method with calcinations to aim at obviously reducing the total fabrication time. The synthesized samples showed integrated structures and good electrochemical performance which were investigated in detail.

2. EXPERIMENTAL

2.1 Materials preparation

$NiSO_4 \cdot 6H_2O$, $CoSO_4 \cdot 7H_2O$ and $MnSO_4 \cdot H_2O$ as the starting materials were dissolved in deionized water with the mole ratio of 1:1:1 and formed an aqueous solutions with the concentration of 2.0 $mol \cdot L^{-1}$. The appropriate amounts of NH_4OH solution as a chelating agent was slowly pumped into

the aqueous solution to make the NH^{4+} and M^{2+} (M = Ni, Co, Mn) mixed sufficiently. Then a 4.0 $mol \cdot L^{-1}$ NaOH solution was added with the ever-increasing stirring rate until pH = 11 was reached. The mixed suspension was stirred at room temperature for 0.5 h and then transferred to a 100 ml Teflon beaker autoclave. The autoclave was heated up to 200 °C and kept the temperature for 5 h and then cooled to room temperature naturally. The precursor powders were obtained through filtering, washing, and drying in a vacuum oven at 80 °C for 12 h to remove adsorbed water. The obtained precursor $Ni_{1/3}Co_{1/3}Mn_{1/3}(OH)_2$ and 5 % excess $LiOH \cdot H_2O$ powders were mixed thoroughly and the mixture was first heated at 450 °C for 2 h and then calcined at 850 °C for 4, 6, 8, 10 and 12 h respectively in air to obtain $LiNi_{1/3}Co_{1/3}Mn_{1/3}O_2$ powders. The corresponding samples were referred as A, B, C, D and E. The synthesis process of $LiNi_{1/3}Co_{1/3}Mn_{1/3}O_2$ powders was shown in Fig. 1.

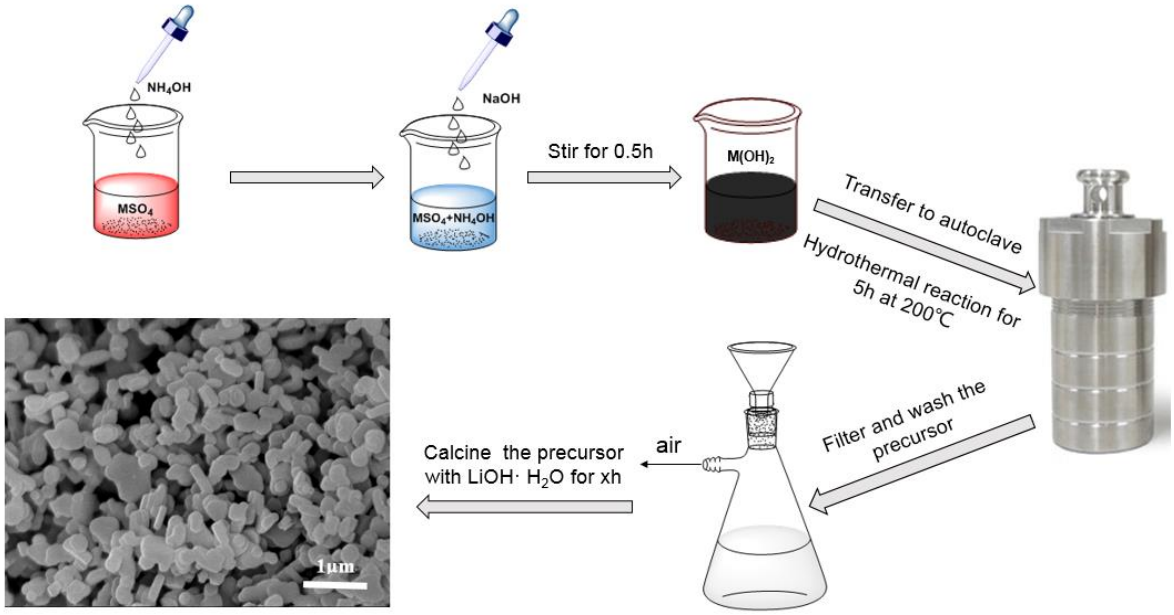

Figure 1. Schematic representation of synthesizing $LiNi_{1/3}Co_{1/3}Mn_{1/3}O_2$ powders.

2.2 Structure and morphology characterizations

X-ray diffraction (XRD) measurement was carried out using Cu target Kα (λ=1.5418 Å) radiation in the 2 θ range of 10 - 80 ° with a step size of 0.06 $° \cdot s^{-1}$. The morphologies and surface microanalysis of the prepared powders were observed using scanning electron microscope (SEM) (JSM-6490LV and JSM-7500F) with the energy disperse spectroscopy (EDS) (51-XMX0019).

The valence states of the transition metals in $LiNi_{1/3}Co_{1/3}Mn_{1/3}O_2$ were measured in a vacuum condition and this operation was finished by X-ray photoelectron spectroscopy (XPS) (KRATOS MSAM-800).

2.3 Electrochemical performance measurements

The electrochemical characterizations were performed using a CR 2025 coin-type cell. The cell consisted of a positive electrode and a lithium metal anode separated by a PP-PE-PP separator. The

positive electrode, prepared by blending 80 wt % $LiNi_{1/3}Co_{1/3}Mn_{1/3}O_2$ active materials, 10 wt % acetylene black and 10 wt % PVDF with the dispersing agent of NMP, was coated onto an aluminum foil current collector. The electrolyte was 1 $mol \cdot L^{-1}$ LiPF6 with EC + DMC (1:1 in volume). All cells were assembled in an Argon-filled glove box.

Cycling and rate tests were performed at a constant current with voltage between 2.7 to 4.5 V at 25 °C using CT2001A Land instrument. The cyclic voltammetry (CV) tests were operated on PARSTAT 2273 electrochemical workstation at 0.1 $mv \cdot s^{-1}$ between 2.7 V to 4.5 V. The electrochemical impedance spectroscopy (EIS) measurements were also performed by the same instrument, using an amplitude voltage of 5 mV and frequency range from 1 MHz to 5 mHz.

3. RESULTS AND DISCUSSION

3.1 Structure and morphology

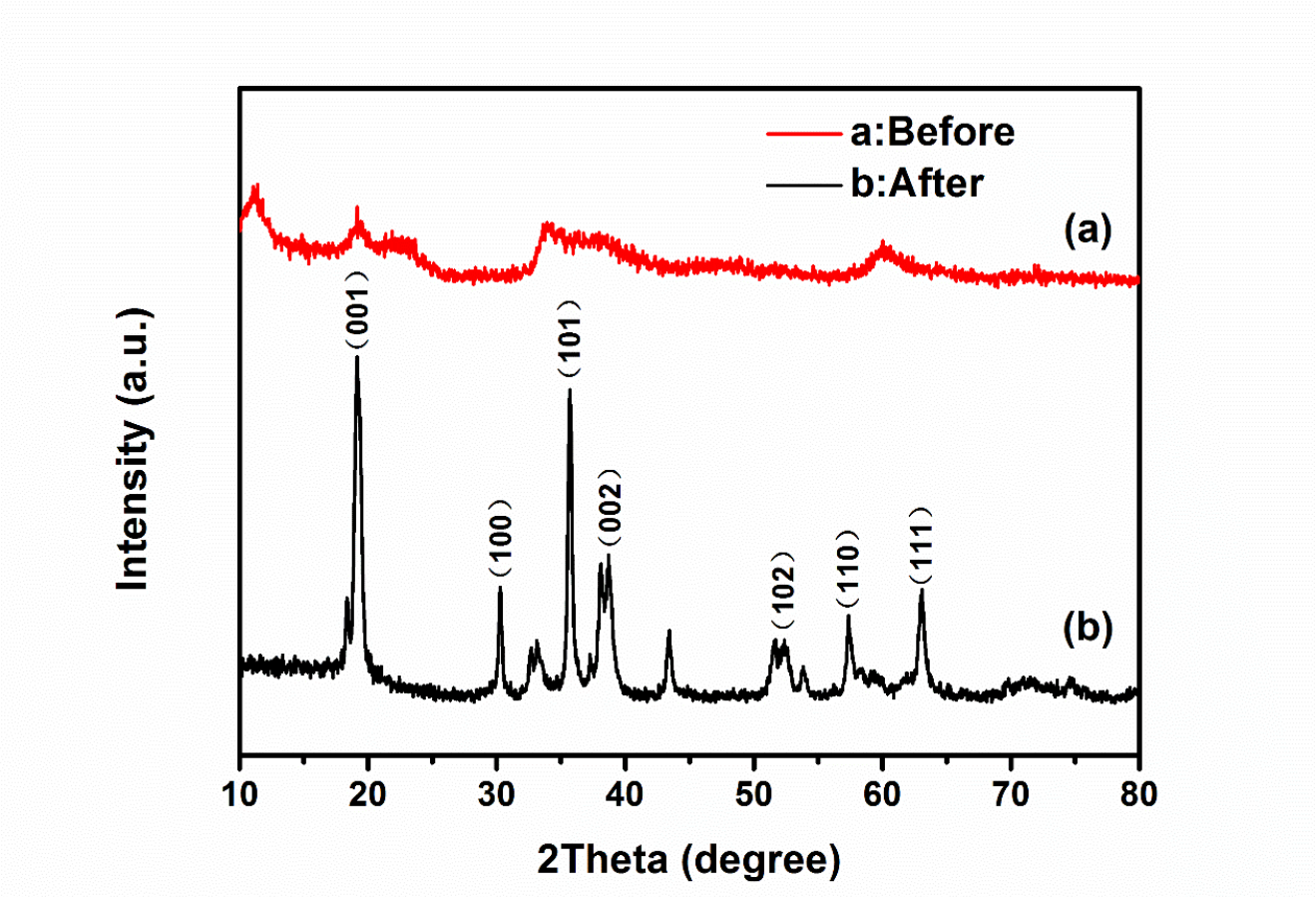

Figure 2. XRD patterns of precursor powders: (a) before hydrothermal treatment; (b) after hydrothermal treatment.

The XRD patterns of precursor powders before and after hydrothermal treatment are shown in Fig. 2. and the peaks of spectrogram (b) are indexed on the basis of $Ni(OH)_2$ (JCPDS 14-0117), $Co(OH)_2$ (JCPDS 30-0443) and $Mn(OH)_2$ (JCPDS 12-0696) structures. The enormous differences between (a) and (b) can be directly observed. After hydrothermal treatment, the precursor owes sharper

and narrower diffraction peaks as well as higher intensity. It is reasonable to deduce that the hydrothermal treatment is beneficial to crystallize well. Moreover, both of the two precursors in the XRD patterns show broad integrated diffraction lines. This can be attributed to the mixture of transition metal carbonates such as $Ni(OH)_2$, $Co(OH)_2$ and $Mn(OH)_2$ [26, 27].

Fig. 3(a) and (b) show the morphology of the hydrothermally treating precursor at different magnification. It is obvious that the primary particles are relatively fine and homogeneous with the size of about 100 nm. The EDS result of Fig. 3(d) corresponding to Fig. 3(c) indicates that the molar ratio of Ni:Co:Mn in precursor prepared by hydrothermally-assisted co-precipitation method is 1:0.96:0.95, which is very close to the initial ingredient (Ni:Co:Mn = 1:1:1). In addition, the mapping patterns in Fig. 3(e), (f) and (g) exhibit the homogeneous distribution of Ni, Co and Mn three elements.

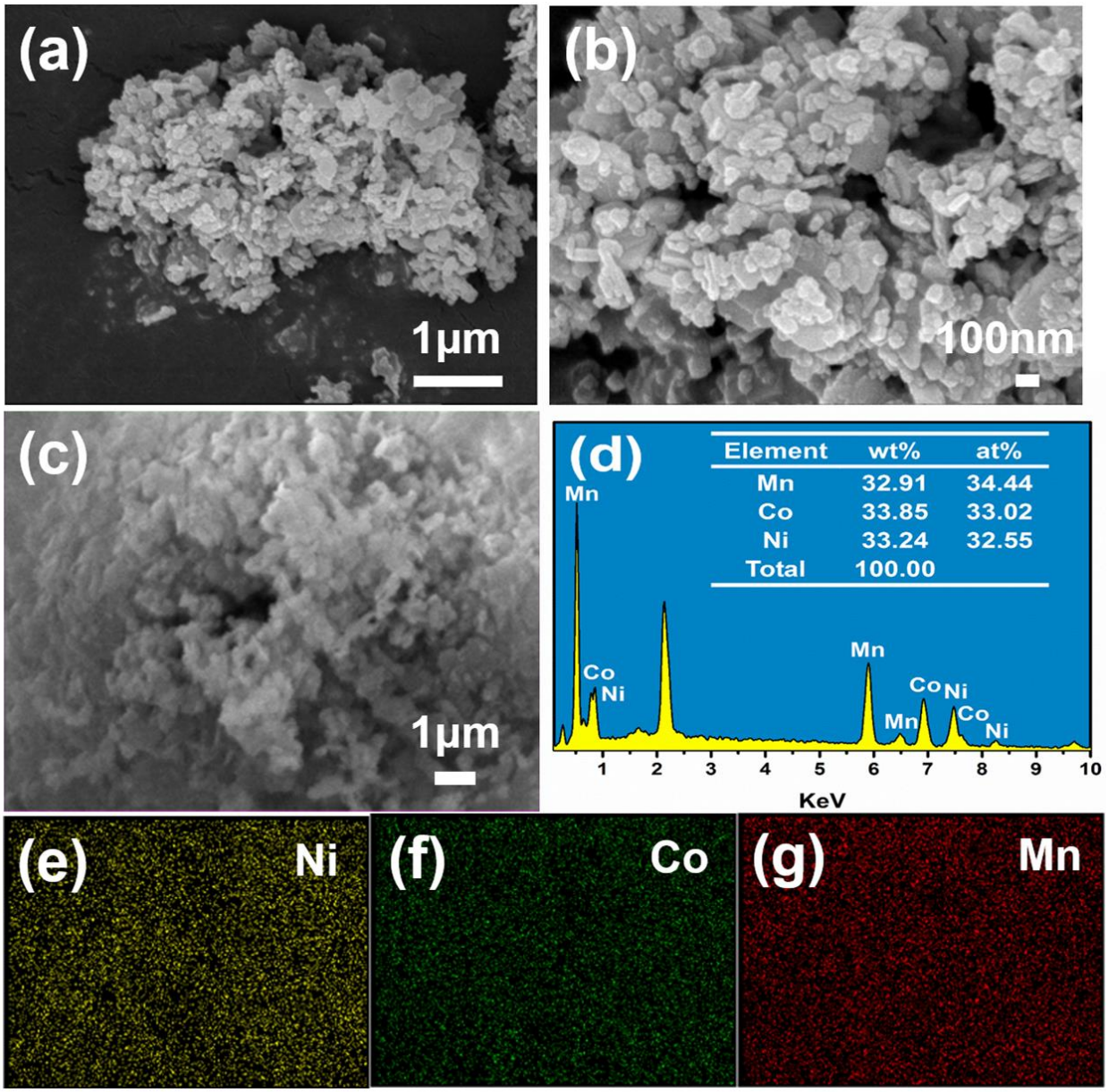

Figure 3. SEM images of precursor powders: (a) × 20000; (b) × 50000. (c) EDS profiles, (d) metal contents, (e-g) mapping figures of the precursor materials along with an SEM.

Fig. 4 shows the X-ray powder diffraction patterns of the $LiNi_{1/3}Co_{1/3}Mn_{1/3}O_2$ powders calcined at 850 °C for different hours. Compared with the hydrothermally treating precursor, the crystallinity of the $LiNi_{1/3}Co_{1/3}Mn_{1/3}O_2$ materials has been enhanced. The obtained powders have the same α-$NaFeO_2$ type layered structure with a $R\bar{3}m$ space group and exhibit the single-phase $LiNi_{1/3}Co_{1/3}Mn_{1/3}O_2$ without any impurity phase [19, 28]. In the α-$NaFeO_2$ type structure, the (006)/(102) and (108)/(110) in the XRD patterns characterizes the layered structure. In Fig. 4, the obvious peak splits in the (006)/(102) and (108)/(110) in all samples indicate the typical layered structures. The integrated intensity ratio (R) of (003)/(104) crystal planes indirectly indicates the mixing extent of cation Li^+ (0.76 Å) and Ni^{2+} (0.69 Å) in the lithium layer [29]. Usually, the higher the ratio of *I*(003)/*I*(104), the lower the cation mixing degree of Li^+ and Ni^{2+} and R = 1.2 is considered to be the boundary [19]. For the prepared materials A - E in Fig. 4, all of the *I*(003)/*I*(104) ratios are higher than 1.2, which prove that the $LiNi_{1/3}Co_{1/3}Mn_{1/3}O_2$ synthesized by hydrothermal assisting co-precipitation has a low degree of cation mixing. As a result, the best calcination time is 8 hours at 850 °C for the hydrothermally-assisted treating precursor.

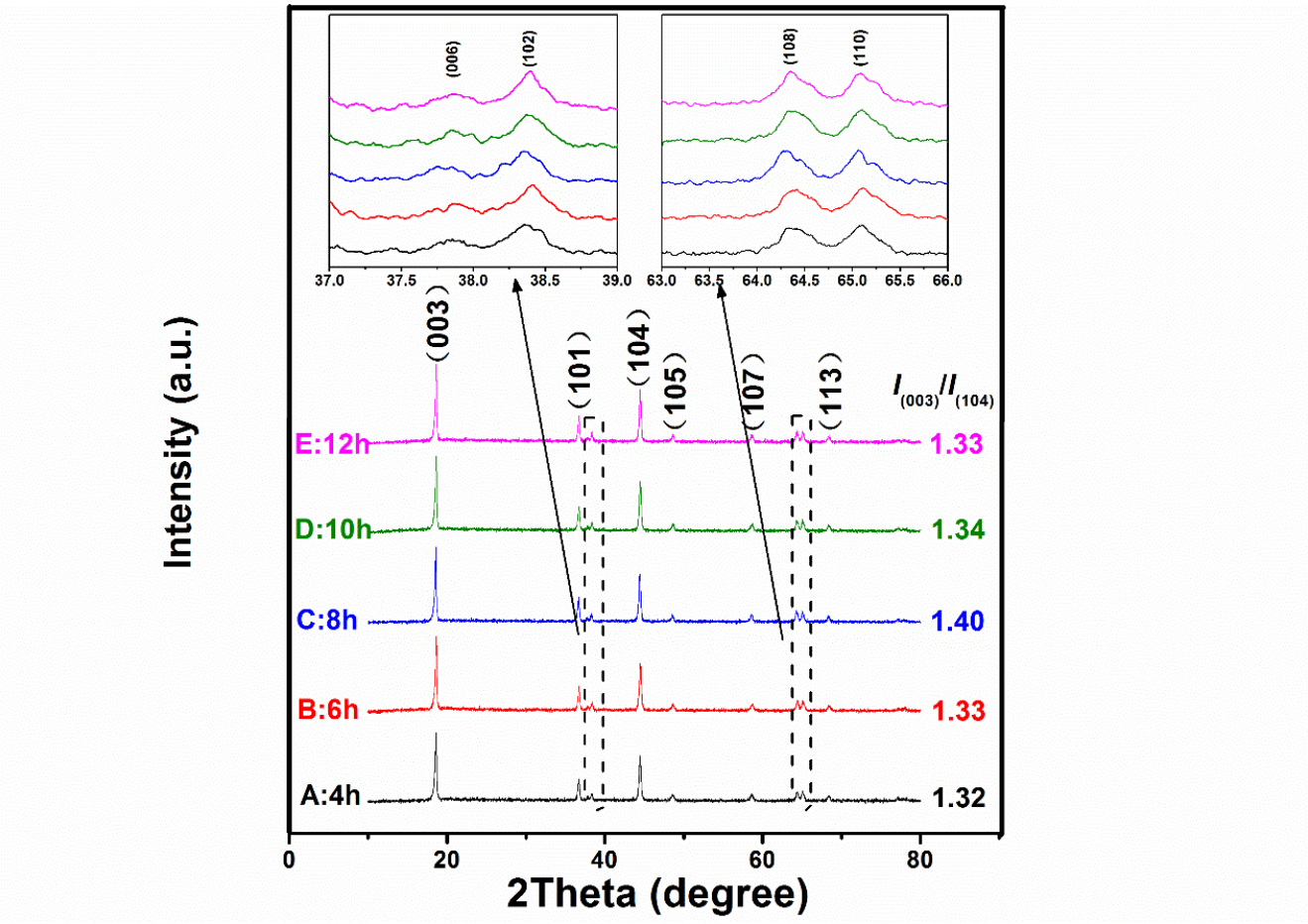

Figure 4. XRD patterns of $LiNi_{1/3}Co_{1/3}Mn_{1/3}O_2$ powders with different calcination hours: (A) 4 h; (B) 6 h; (C) 8 h; (D) 10 h; (E) 12 h.

The SEM images of the $LiNi_{1/3}Co_{1/3}Mn_{1/3}O_2$ are showed in Fig. 5. After calcination, the particle sizes of $LiNi_{1/3}Co_{1/3}Mn_{1/3}O_2$ increase distinctly. All of the particles are short rod-like. In the

sample A with a short calcination time of 4 h, the smaller particles adhere to the bigger one, which is due to an incomplete reaction. The agglomeration appears in the sample E with a long calcination time of 12 h. Comparatively speaking, the sample C calcined for 8 h is deemed the optimal materials with clearly visible particle edges and average particle size of 300 nm.

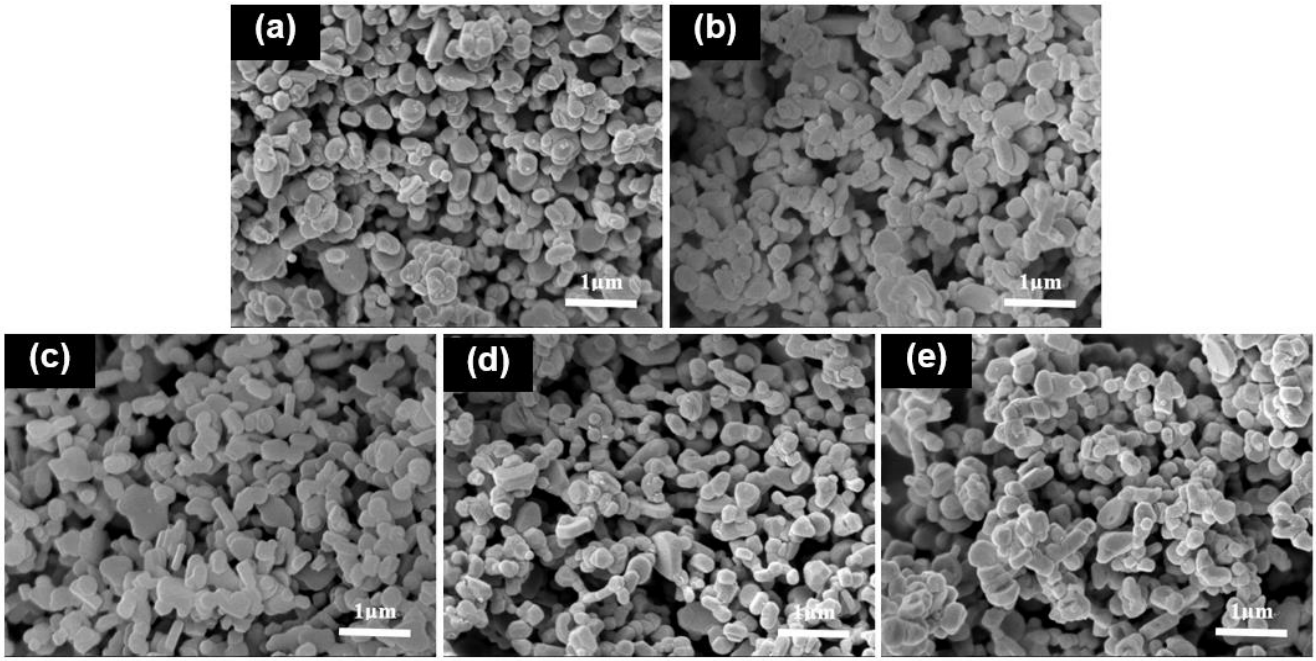

Figure 5. SEM images of $LiNi_{1/3}Co_{1/3}Mn_{1/3}O_2$ powders with different calcination hours: (a) 4 h; (b) 6 h; (c) 8 h; (d) 10 h; (e) 12 h.

X-ray photoelectron spectroscopy (XPS) measurement was performed to determine the valence state of nickel, cobalt and manganese, and the detailed results are presented in Fig. 6. The binding energy of C 1s (284.6 eV, shown in Fig. 6(f)) is chosen to be the calibration for all the other spectra in XPS analysis. From the wide scan spectrum in Fig. 6(a) it can be clearly seen that all of needed elements Ni, Co, Mn, O and C are checked. By using the Gaussian fitting method, the Ni 2p XPS spectra are shown in Fig. 6(b). The two dominant peaks located at 872.3 and 854.7 eV are characteristic of Ni^{2+} corresponding to Ni $2p_{1/2}$ and Ni $2p_{3/2}$ with a spin-energy separation of ~17.6 eV [30]. And the two shake-up satellite peaks around 879.2 and 861.1 eV can further confirm the existence of Ni^{2+}. Moreover, there are no signals of Ni^{3+} [31-34]. The Co 2p spectrum has two main peaks in Fig. 6(c), 794.7 eV for $2p_{1/2}$ and 779.7 eV for $2p_{3/2}$ with a spin-orbital splitting of ~15.0 eV, corresponding to a Co^{3+} state [35, 36]. By XPS curve fitting, the co-existence of Co^{4+} is suggested with the peaks appearing at 781.0 and 796.2 eV respectively [31, 35]. While there are no obvious satellite peaks at 785.0 - 788.0 eV range, indicating the inexistence of Co^{2+} [35, 36]. As shown in Fig 6 (d), there are two major peaks in the Mn 2p spectrum, $2p_{1/2}$ at 653.9 eV and $2p_{3/2}$ at 642.5 eV with a separation ~11.4 eV corresponding to Mn^{4+} cation. In addition, an auger peaks is found at 636.9 eV. Fig. 6(e) is the XPS spectrum of oxygen.

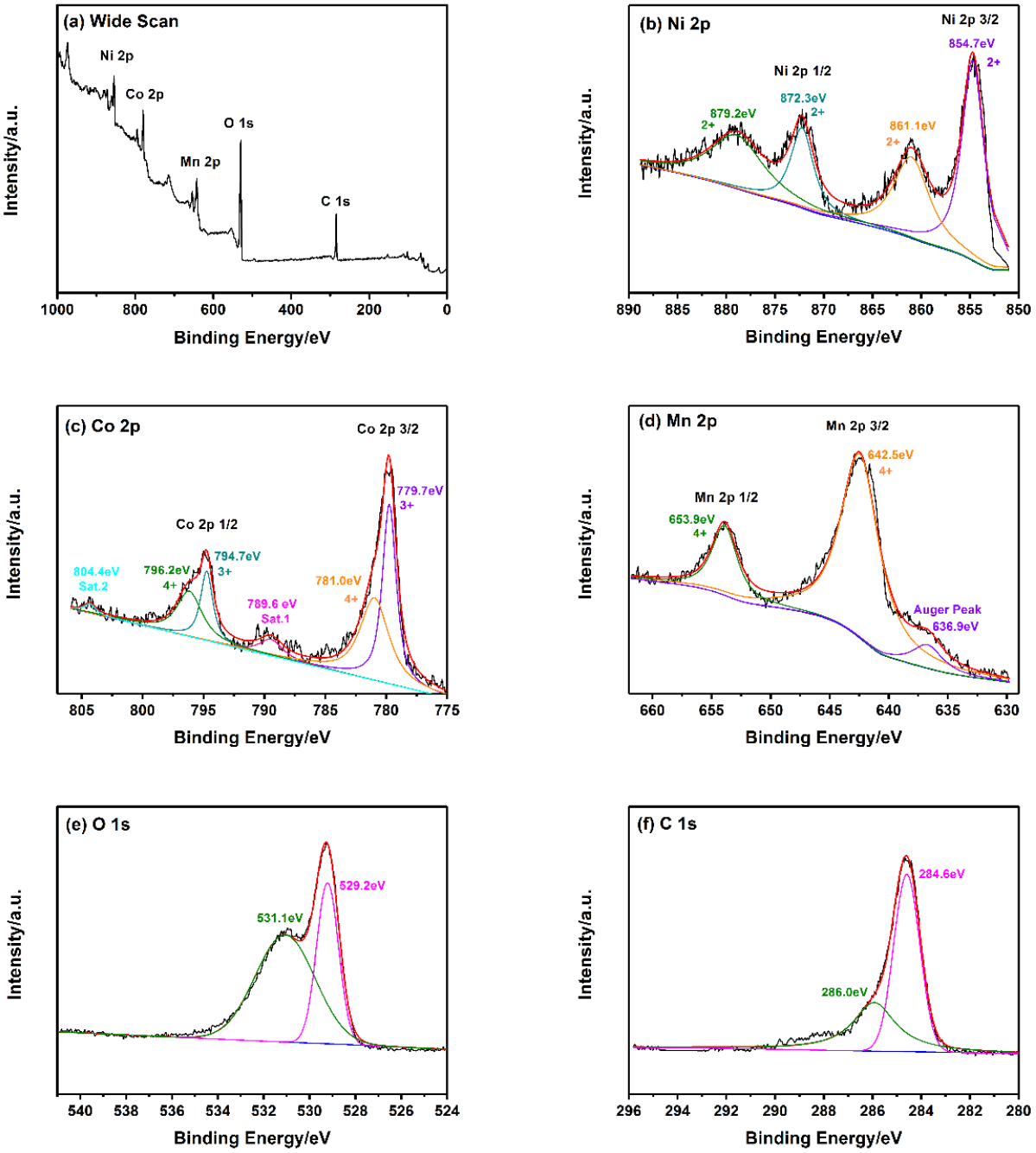

Figure 6. XPS spectra of (a) a wide scan, (b) Ni 2p, (c) Co 2p, (d) Mn 2p, (e) O 1s, (f) C 1s of $LiNi_{1/3}Co_{1/3}Mn_{1/3}O_2$ powders.

3.2 Electrochemical performance

The initial charge–discharge curves of the prepared $LiNi_{1/3}Co_{1/3}Mn_{1/3}O_2$ between 2.7 and 4.5 V at a current density of 0.1 C are showed in Fig. 7(a). The sample A calcined for 4 h shows the initial charge capacity of 190.5 $mAh \cdot g^{-1}$ and the discharge capacity of 155.4 $mAh \cdot g^{-1}$. With the heat treatment increased to 6 h (B), 8 h (C), 10 h (D) and 12 h (E), the charge capacities are 201.7 $mAh \cdot g^{-1}$,

229.5 mAh·g^{-1}, 219.9 mAh·g^{-1} and 261.3 mAh·g^{-1} respectively. The corresponding discharge capacities are 163.5 mAh·g^{-1} (B), 193.5 mAh·g^{-1} (C), 177.7 mAh·g^{-1} (D) and 214.0 mAh·g^{-1} (E). The decomposition of electrolyte and the formation of a solid electrolyte interface (SEI) on the surface are the main reasons for irreversible capacity loss [18]. The discharge capacity of 8 h calcined sample C is a little lower than that of 12 h calcined sample E.

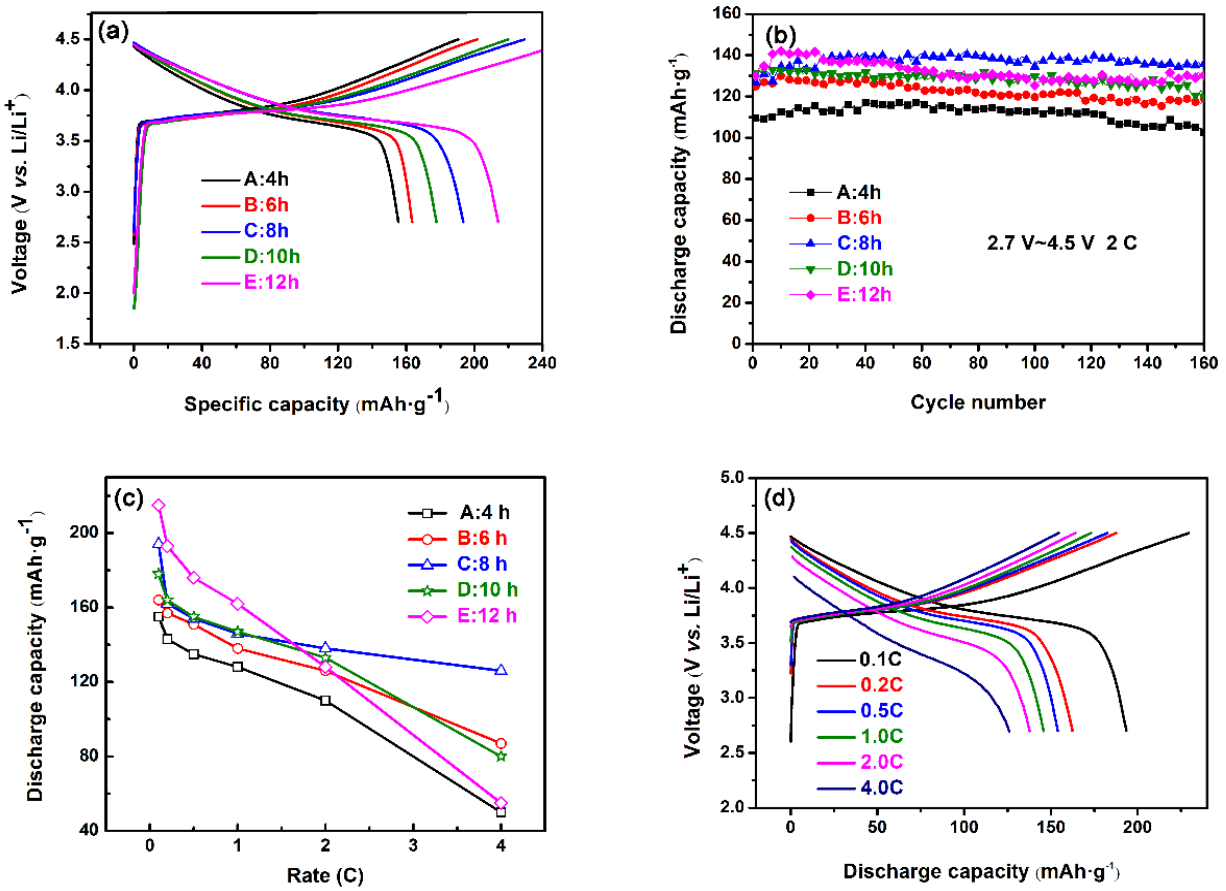

Figure 7. Electrochemical characterization of $LiNi_{1/3}Co_{1/3}Mn_{1/3}O_2$ electrode as the cathode of lithium-ion batteries: (a) initial charge-discharge curves at 0.1 C; (b) cycling performance at 2.0 C; (c) rate capability with different calcination hours: (A) 4 h, (B) 6 h, (C) 8 h, (D) 10 h, (E) 12 h. (d) Rate capability of sample C.

The discharge capacity vs cycle number of $LiNi_{1/3}Co_{1/3}Mn_{1/3}O_2$ is illustrated in Fig. 7(b). The tests were performed at a constant current density of 2.0 C and cycled between 2.7 to 4.5 V. After 135 times cycles, the capacity retentions of each sample are 88.95 % (A), 89.08 % (B), 97.79 % (C), 93.59 % (D) and 89.58 % (E) respectively, based on their largest discharge capacities. The results indicate that all of the samples possess good cycling performance. The sample C shows the highest discharge capacity and capacity retention.

Fig. 7(c) reflects the rate capacity of $LiNi_{1/3}Co_{1/3}Mn_{1/3}O_2$. The samples were charged to 4.5 V and then discharged to 2.7 V at 0.1 C, 0.2 C, 0.5 C, 1.0 C, 2.0 C and 4.0 C. With the discharge current density increasing, the discharge capacity decrease because of polarization. The discharge capacities

are 155 $mAh \cdot g^{-1}$ (A), 164 $mAh \cdot g^{-1}$ (B), 194 $mAh \cdot g^{-1}$ (C), 178 $mAh \cdot g^{-1}$ (D) and 215 $mAh \cdot g^{-1}$ (E), respectively at 0.1 C and reduce to 50 $mAh \cdot g^{-1}$ (A), 87 $mAh \cdot g^{-1}$ (B), 126 $mAh \cdot g^{-1}$ (C), 80 $mAh \cdot g^{-1}$ (D) and 55 $mAh \cdot g^{-1}$ (E), respectively at 4.0 C. The 8 h calcined sample C has the best rate capacity with the highest discharge capacity of 126 $mAh \cdot g^{-1}$ at large current density of 4.0 C and the minimal influence of polarization, which is also clearly showed in Fig. 7(d). It is reasonable that the less cation mixing is beneficial for electrochemical performance.

The comparisons among the reported articles [20, 22-24, 26] and our work are enumerated in the Table 1. It is very obvious that the hydrothermally-assisted co-precipitation method requires much shorter precursor reaction and calcination time than single co-precipitation method. In Table 1, the total fabrication time is 15 h for the $LiNi_{1/3}Co_{1/3}Mn_{1/3}O_2$ prepared by hydrothermally-assisted method while at least about 27 h or longer for that prepared by co-precipitation method. The calcination temperature is 900 °C in the article [22] and [24] as well as 950 °C in the articles [20] but the calcination temperature is only 850 °C for the hydrothermally-assisted precursor in this work. Besides, the hydrothermally-assisted $LiNi_{1/3}Co_{1/3}Mn_{1/3}O_2$ has the largest initial discharge capacity of 193.5 $mAh \cdot g^{-1}$, its capacity fading rate per cycle is only 0.016 % while their capacity fading rates per cycle are from 0.052 % to 0.118 % for all of the $LiNi_{1/3}Co_{1/3}Mn_{1/3}O_2$ materials through co-precipitation method. In summary, the hydrothermally-assisted co-precipitation method can shorten obviously the fabrication time of the $LiNi_{1/3}Co_{1/3}Mn_{1/3}O_2$ material, which is helpful to boost the utilization of production equipments and reduce the manufacturing cost of the $LiNi_{1/3}Co_{1/3}Mn_{1/3}O_2$ material.

Table 1. Summary of the electrochemical performance of previous lithium-ion batteries based on $LiNi_{1/3}Co_{1/3}Mn_{1/3}O_2$ cathodes compared to this work

Method	Precursor Reaction temperature and time	Calcination temperature and time	Total fabrication time	Initial discharge capacity /($mAh \cdot g^{-1}$)	Capacity fading rate per cycle	Refs
Hydrothermal method	160 °C / 30 h	850 °C / 6 h	36 h	187.7 (20 $mA \cdot g^{-1}$)	0.053 %	[26]
Carbonate co-precipitation		900 °C / 20 h	> 20h	170.0 (16 $mA \cdot g^{-1}$)	0.118 %	[22]
Carbonate co-precipitation	60 °C / 12 h	500 °C / 5 h 850 °C / 12 h	29 h	162.7 (32 $mA \cdot g^{-1}$)	0.052 %	[23]
Hydroxide co-precipitation	60 °C / 12 h	950 °C / 15 h	27 h	163.0 (20 $mA \cdot g^{-1}$)	0.076 %	[20]

Hydroxide co-precipitation	50 °C / 24 h	400 °C / 6 h 900 °C / 12 h	42 h	148.0 (160 mA·g^{-1})	0.100%	[24]
Hydrothermally-assisted co-precipitation method	25 °C / 0.5 h 200 °C / 5.0 h	450 °C / 2 h 850 °C / 8 h	15.5 h	193.5 (18.3 mA·g^{-1})	0.016 %	This work

3.3 Cyclic voltammetry (CV)

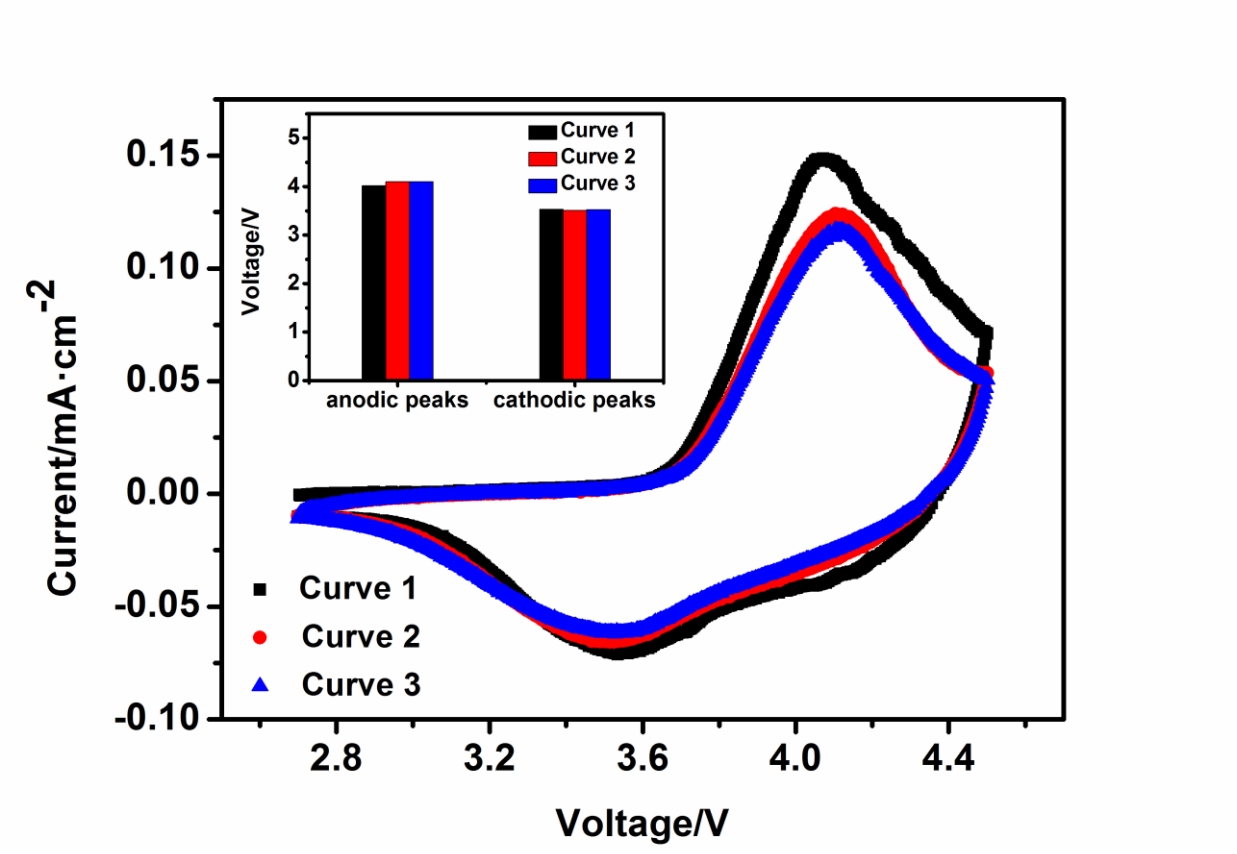

Figure 8. Cyclic voltammetry of sample C between 2.7 and 4.5 V at a scan rate of 0.1 mV·s^{-1}.

In order to further explore the process of charge-discharge and the electrode polarization, we tested the cyclic voltammetry of the 8 h calcined sample C. The first three cycles of sample C between 2.7 and 4.5 V at a scan rate of 0.1 mV·s^{-1} is shown in Fig. 8. We could see from the first cycle that the anodic peak is located at 4.07 V and the cathodic peak at 3.53 V, which are corresponding to the Ni^{2+}/Ni^{4+}. The electrochemical reactions of the charging process can be described as: [37]

$LiNi_{1/3}Co_{1/3}Mn_{1/3}O_2 \underset{\text{discharge}}{\overset{\text{charge}}{\rightleftharpoons}} Li_{1-x}(Ni^{2+}_{1/3-x}Ni^{3+}_{x})Co_{1/3}Mn_{1/3}O_2 + x\ Li^+ + x\ e^-$ ($0 \le x \le 1/3$, 3.8 - 4.1V) (1)

$Li_{2/3}Ni^{3+}_{1/3}Co_{1/3}Mn_{1/3}O_2 \underset{\text{discharge}}{\overset{\text{charge}}{\rightleftharpoons}} Li_{1-x}(Ni^{3+}_{2/3-x}Ni^{4+}_{x-1/3})Co_{1/3}Mn_{1/3}O_2 + (x-1/3)\ Li^+ + (x-1/3)\ e^-$ ($1/3 \le x \le 2/3$, 3.8 - 4.1 V) (2)

After the first cycle, the curves of the second and third cycle are almost overlapped. The voltage values of anodic peaks and cathodic peaks corresponding to the curve 2 and 3 are shown in Fig.8, and the ΔV are 0 V for anodic peaks and 0.014 V for cathodic peaks respectively, indicating that the electrode has a stable structure and a good reversibility. However, the intensity of the two anodic peaks slightly decrease than that of the first curve, owing to the irreversible capacities after the first cycle.

3.4 Electrochemical impedance spectroscopy (EIS)

Electrochemical impedance spectroscopy (EIS) was applied to study the Li^+ ions diffusion. Fig. 9(a) is the EIS comparisons of $LiNi_{1/3}Mn_{1/3}Co_{1/3}O_2$ cells with different calcination hours and the impedance results are fitted by the same equivalent circuit. At the Z' axis, a high-frequency intercept is mainly the electrolyte (Re). The curves contain a high-frequency semi-circle and a slash at the low frequency [38, 39]. The former represents the solid electrolyte interface resistance (R_{SEI}) and the charge transfer resistance (R_{ct}) between the electrolyte and electrode, while the latter exhibits diffusion of Li^+ in the electrode, i.e. Warburg impedance (W), respectively. As shown in Fig. 9(a), the overall impedance decreases first and then increases with calcination time extension and the 8 h is the turning point, illustrated by the size changes of the semi-circles. The statistical datas of Re and R_{SEI} + R_{ct} in Table 2 further confirm the result. The lithium-ion diffusion coefficient D ($cm^2 \cdot s^{-1}$) can be calculated from the formula on the basis of EIS diagram as following: [40, 41]

$$D=R^2T^2/2A^2n^4F^4C^2\sigma^2 \quad (3)$$

where R means the gas constant (8.314 $J \cdot mol^{-1} \cdot K^{-1}$), T is the room temperature (298 K), A represents the surface area of the electrode, n is the number of the electrons per molecule during the electronic transfer reaction (1), F is the Faraday constant (96485 $C \cdot mol^{-1}$), C is the concentration of lithium-ion in $LiNi_{1/3}Mn_{1/3}Co_{1/3}O_2$ electrode, and σ is the slope of the line $Z' \sim \omega^{-1/2}$, which was shown in the Fig. 9(b) - (f). The calculated results in Table 2 indicate that the lithium-ion diffusion coefficient D increases first and then decrease with the calcination time from 4 h to 12 h. The sample C calcined for 8 h has the highest diffusion coefficient of 5.382×10^{-15} $cm^2 \cdot S^{-1}$, meaning the fastest charge-transfer process. This result is consistent with the outstanding electrochemical performance of sample C mentioned above. The lithium-ion diffusion coefficients of sample D and E are lower than A, B and C for two orders of magnitude, which corresponding to the poor rate capacities and large resistances of the two samples.

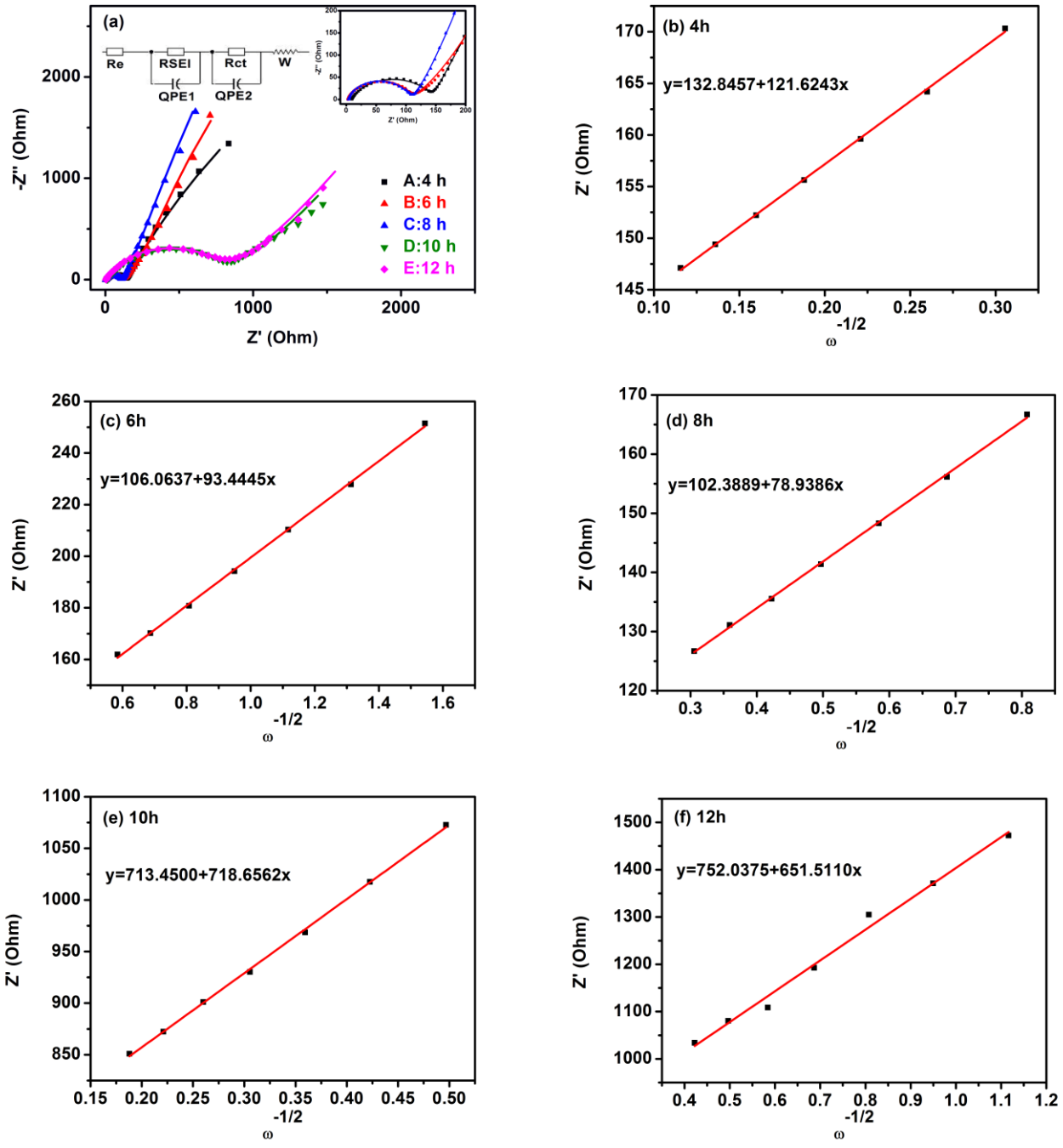

Figure 9. (a) The comparison of EIS of $LiNi_{1/3}Mn_{1/3}Co_{1/3}O_2$ cells with different calcination hours: (A) 4 h, (B) 6 h, (C) 8 h, (D) 10 h, (E) 12 h. Slope fitted curves of (b) 4h; (c) 6h; (d) 8h; (e) 10h; (f) 12h.

Table 2. The resistance and lithium-ion diffusion coefficient in cathode at different calcination hours

Sample	R_e / Ω	$R_{SEI} + R_{ct}$ / Ω	D_{Li+} / ($cm^2 \cdot S^{-1}$)
A: 4 h	8.4295	132.9114	1.646×10^{-15}
B: 6 h	2.7010	110.9012	2.381×10^{-15}
C: 8 h	3.8227	104.5124	5.382×10^{-15}
D: 10 h	12.5693	811. 2186	2.896×10^{-17}
E: 12 h	6.0083	835.1451	2.730×10^{-17}

4. CONCLUSIONS

Hydrothermally-assisted co-precipitation method is employed to prepare the precursor of layered materials $LiNi_{1/3}Co_{1/3}Mn_{1/3}O_2$. The high-temperature and high-pressure conditions that the hydrothermal-assisted method possesses can rapidly improve the crystallization speed of $LiNi_{1/3}Co_{1/3}Mn_{1/3}O_2$ precursor. As the result, the hydrothermally-assisted co-precipitation method requires much shorter precursor reaction and calcination time and at the same time the good comprehensive electrochemical performance can be obtained. The total fabrication time is 15 hours for the $LiNi_{1/3}Co_{1/3}Mn_{1/3}O_2$ prepared by hydrothermally-assisted method and at least about 27 hours or longer for that prepared by reported co-precipitation methods. Besides the hydrothermally-assisted $LiNi_{1/3}Co_{1/3}Mn_{1/3}O_2$ has the large initial discharge capacity of 193.5 $mAh \cdot g^{-1}$ and good high-rate capacity of 126 $mAh \cdot g^{-1}$ at 4.0 C, its capacity fading rate per cycle is only 0.016 % which is much lower than that reported through co-precipitation methods. Adopting the hydrothermally-assisted co-precipitation method is very helpful to boost the utilization of production equipments and reduce the manufacturing cost of the $LiNi_{1/3}Co_{1/3}Mn_{1/3}O_2$ material.

ACKNOWLEDGEMENTS
This work was financially supported by the Research Project of Baosheng Industrial Development Co., Ltd. [Grant No. 15H1107].

References

1. K. Mizushima, P. C. Jones, P. J. Wiseman and J. B. Goodenough, *Mater. Res. Bull.*, 15 (1980) 783.
2. J. B. Goodenough and K. Mizuchima, *US 4302518*, (1981).
3. R. Koksbang, J. Barker, H. Shi and M. Y. Saïdi, *Solid State Ion.*, 84 (1996) 1.
4. J. M. Tarascon, E. Wang, F. K. Shokoohi, W. R. McKinnon and S. Colson, *J. Electrochem. Soc.*, 138 (1991) 2859.
5. Y. Xia and M. Yoshio, *J. Electrochem. Soc.*, 143 (1996) 825.
6. A. K. Padhi, J. B. Goodenough and K. S. Nanjundaswamy, *J. Electrochem. Soc.*, 144 (1997) 1188.
7. A. Yamada, S. C. Chung and K. Hinokuma, *J. Electrochem. Soc.*, 148 (2001) A224.
8. L. Xiao, Y. Yang, Y. Zhao, X. Ai, H. Yang and Y. Cao, *J. Solid State Electrochem.*, 12 (2008) 149.
9. T. E. Hong, E. D. Jeong, S. R. Baek, M. R. Byeon, Y. S. Lee, F. N. Khan and H. S. Yang, *J. Appl. Electrochem.*, 42 (2012) 41.
10. R. Thirunakaran, T. Kim and W. S. Yoon, *J. Appl. Electrochem.*, 44 (2014) 709.
11. Y. Shin and A. Manthiram, *J. Electrochem. Soc.*, 151 (2004) A204.
12. G. D. Bent, G. F. Adams, R. H. Bartram, G. D. Purvis and R. J. Bartlett, *J. Chem. Phys.*, 13 (1982) 4144.
13. X. Fang, J. Li, K. Huang, S. Liu, C. Huang, S. Zhuang and J. Zhang, *J. Solid State Electrochem.*, 16 (2012) 767.
14. W. Su, K. Xu, G. Zhong, Z. Wei, C. Wang and Y. Meng, *Int. J. Electrochem. Sci.*, 12 (2017) 6930.
15. K. M. Shaju and P. G. Bruce, *Adv. Mater.*, 18 (2006) 2330.
16. J. B. Goodenough and Y. Kim, *Chem. Mater.*, 22 (2010) 587.
17. W. Hua, Y. Wang, Y. Zhong, G. Wang, B. Zhong, B. Fang and X. Guo, *Chin. J. Chem.*, 33 (2015) 261.
18. K. M. Shaju, G. S. Rao and B. V. R. Chowdari, *Electrochim. Acta*, 48 (2002) 145.

19. M. H. Lee, Y. J. Kang, S. T. Myung and Y. K. Sun, *Electrochim. Acta*, 50 (2004) 939.
20. H. J. Noh, S. Youn, S. Y. Chong and Y. K. Sun, *J. Power Sources*, 233 (2013) 121.
21. F. Fu, G. L. Xu, Q. Wang, Y. P. Deng, X. Li, J. T. Li, L. Huang and S. G. Sun, *J. Mater. Chem. A.*, 1 (2013) 3860.
22. S. H. Park, S. H. Kang, I. Belharouak, Y. K. Sun and K. Amine, *J. Power Sources*, 177 (2008) 177.
23. S. Zhang, C. Deng, B. L. Fu, S. Y. Yang and L. Ma, *Powder Technol.*, 198 (2010) 373.
24. R. Santhanam and B. Rambabu, *J. Power Sources*, 195 (2010) 4313.
25. J. Fan, G. Li, D. Luo, C. Fu, Q. Li, J. Zheng and L. Li, *Electrochim. Acta.*, 173 (2015) 7.
26. F. Wu, M. Wang, Y. Su, L. Bao and S. Chen, *J. Power Sources*, 195 (2010) 2362.
27. T. H. Cho, S. M. Park, M. Yoshio, T. Hirai and Y. Hideshima, *J. Power Sources*, 142 (2005) 306.
28. K. W. Nam, S. M. Bak, E. Hu, X. Yu, Y. Zhou, X. Wang, L. Wu, Y. Zhu, K. Y. Chung and X. Q. Yang, *Adv. Funct. Mater.*, 23 (2013) 1046.
29. S. C. Yin, Y. H. Rho, I. Swainson and L. F. Nazar, *Chem. Mater.*, 18 (2006) 1901.
30. J. Liang, R. Ma, N. Iyi, Y. Ebina, K. Takada and T. Sasaki, *Chem. Mater.*, 22 (2010) 371.
31. C. Zhen, W. Jin, D. Chao, B. Tom, L. Bai, C. Shi, Y. Zhao, S. T. Chien, J. Lin and Z. Shen, *Sci. Rep.*, 6 (2016) 25771.
32. M. Li, J. P. Cheng, F. Liu and X. B. Zhang, *Chem. Phys. Lett.*, 640 (2015) 5.
33. L. Gu, L. Qian, Y. Lei, Y. Wang, J. Li, H. Yuan and D. Xiao, *J. Power Sources*, 261 (2014) 317.
34. J. W. Lee, T. Ahn, D. Soundararajan, J. M. Ko and J. D. Kim, *Chem. Commun.*, 47 (2011) 6305.
35. M. O'Connell, A. K. Norman, C. F. Hüttermann and M. A. Morris, *Catal. Today*, 47 (1999) 123.
36. B. Liu, Y. Zhang and L. Tang, *Int. J. Hydrogen Energy*, 34 (2009) 435.
37. Y. Koyama, I. Tanaka, H. Adachi, Y. Makimura and T. Ohzuku, *J. Power Sources*, 119 (2003) 644.
38. K. M. Shaju, G. V. S. Rao, B. V. R. Chowdari, *J. Electrochem. Soc.*, 151 (2004) A1324.
39. J. Li, R. Yao and C. Cao, *ACS Appl. Mat. Interfaces*, 6 (2014) 5075.
40. L. Wang, J. Zhao, X. He, J. Gao, J. Li, C. Wan and C. Jiang, *Int. J. Electrochem. Sci.*, 7 (2012) 345.
41. X. Wang, H. Hao, J. Liu, T. Huang and A. Yu, *Electrochim. Acta*, 56 (2011) 4065